



Catalytic performance of carbon-supported mixed MoW carbides for the deoxygenation of stearic acid

M. Führer, T. van Haasterecht, J.H. Bitter*

Biobased Chemistry and Technology, Wageningen University, PO Box 17, 6700 AA Wageningen, the Netherlands

ARTICLE INFO

Keywords:

Mixed-metal carbides
Tungsten
Molybdenum
Carbon support
Hydrodeoxygenation

ABSTRACT

Supported bimetallic molybdenum and tungsten carbides are viable replacements for noble metal catalysts and are suitable for the decarboxylation/decarbonylation and (hydro-)deoxygenation of renewable triglyceride-based feedstocks. Here, we show that the Mo:W ratio in bimetallic carbide can steer the product yield towards either aldehydes, alcohols, alkenes or alkanes. The mixed carbides with a higher Mo/W ratio (3:1) reached higher yields of aldehydes and alcohols, while the carbides with a lower Mo/W (1:3) ratio yielded high concentrations of alkenes. Interestingly, a physical mixture of two monometallic (1 + 1) carbides had a similar catalytic performance to the 1:1 mixed carbides. The intrinsic activity (turnover frequency (TOF)) of the catalysts was assessed based on both H₂ and CO chemisorption. The TOF_{H₂} related linearly with the Mo/W ratio, while the TOF_{CO} did not show a relevant relationship. Therefore H₂ chemisorption is suggested as the preferred way to assess the intrinsic activities of these catalysts.

1. Introduction

Transition metal carbides like tungsten and molybdenum carbide display similar or better catalytic activities than noble metals while being less expensive and potentially having a higher tolerance against poisons. [1–4] Since the seminal article of Levy and Boudart in 1973 [5], it became clear that Mo and W carbides are efficient catalysts for reactions that involve hydrogen activation such as hydrogenation [6], hydrodeoxygenation [7] or hydrogenolysis [8]. Lately, also bimetallic carbide catalysts e.g. CoMo-carbide [9], MoNi-carbide [10–13] and CoW-carbide [14] have attracted attention.

For instance, Smirnov et al. [15] used SiO₂ supported NiMo-carbide catalysts with different ratios of Mo₂C and Ni for the hydrodeoxygenation of anisole and for the decarboxylation of ethyl caprate. A positive relation was found between the content of a Ni-Mo alloy and activity for the hydrogenation of anisole. A similar relation was found for the decarboxylation activity of ethyl caprate. Shao et al. [16] and Iyer et al. [17,18] found that unsupported Co₆W₆C catalysts form an active Co-WC phase for the dry reforming of methane to produce syngas. It was stated that these bimetallic carbides had improved activity and stability in comparison to other catalysts that are used for dry reforming (e.g. Ni and Mo₂C).

Also bimetallic Mo and W carbides have recently been used to study a

potential synergetic effect between Mo and W carbides. Tran et al. [19] already showed that in a bulk MoW-carbide system a metallic W phase is present which increased the oxophilicity of the catalysts and increased the number of hydrogen activating sites. The number of sites in the mixed system was higher as expected from mixing the two monometallic carbides. This in turn led to an enhanced hydrodeoxygenation (HDO) activity and resulted in a shift in selectivity. The monometallic Mo₂C was active for both direct deoxygenation (producing benzene) and hydrogenation–dehydration (producing phenol), while the bimetallic MoW carbide strongly favoured the deoxygenation pathway (producing benzene). Fu et al. [20] observed a synergistic effect when combining Mo₂C and W₂C supported on carbon nanotubes for the hydrogen evolution reaction (HER). The mixed carbide with a ratio of 3:1 Mo:W achieved the best electrocatalytic performance in the HER (lowest current density at 0.1 V and Tafel slope of 34 mV/dec) in comparison to the monometallic and the bimetallic mixture of 1:1 and 1:3 Mo:W (Tafel slope of 45–112 mV/dec). This was attributed to a weaker Mo-H_{Abs} bond after the addition of W into the Mo-carbide system.

Motivated by these studies, we investigated bimetallic MoW-carbide catalysts for the hydrodeoxygenation of stearic acid. Monometallic Mo and W carbide catalysts are active for the conversion of stearic (and oleic acid) into alkenes, oxygenates and alkanes following the HDO pathway (Scheme 1). [21–23]. This is in contrast to the noble metals like Pt,

* Correspondence to: Department of Agrotechnology and Food Sciences, Wageningen University and Research, PO Box 17, 6700 AA Wageningen, The Netherlands.
E-mail address: harry.bitter@wur.nl (J.H. Bitter).

which follow under the same reaction conditions the decarboxylation (DCO, dashed blue box in Scheme 1) pathway [22,24]. The HDO pathway involves first the hydrogenation of stearic acid into aldehydes and alcohols i.e., oxygenates and subsequently, the oxygenates can further react via hydrogenation/dehydration yielding alkenes, which in turn can be hydrogenated to the alkanes (blue box in Scheme 1). Interestingly, when comparing carbon-supported Mo-carbides to W-carbides catalysts, the former ones are more selective towards oxygenates at low conversion levels, while the W-carbides are more selective towards alkenes even at high conversions [21]. The differences in intermediate product selectivity between the two carbides can be explained by the more oxophilic nature of W-carbide surface compared to Mo-carbide. [19,21].

In this paper, we want to establish to which extent we can combine the properties of both W-carbide and Mo-carbide by using carbon nanofiber supported mixed MoW-carbides. We will examine how the catalytic performance of mixed MoW carbides depends on the Mo:W ratio. The supported bimetallic carbide catalysts will be prepared by the carbothermal reduction and the hydrodeoxygenation of stearic acid (350 °C, 30 bar of H₂) will be used as test reaction.

2. Material and methods

2.1. Catalyst synthesis

Carbon nanofibers (CNF) were grown from a mixture of hydrogen (102 ml/min), nitrogen (450 ml/min) and carbon monoxide (260 ml/min) at 550 °C and 3 barg for 24 h over a reduced 5 wt% Ni/SiO₂ catalyst (3 g), as reported previously [1]. After synthesis the carbon fibers were treated three times (with intermediate washing with water) with a boiling 1 M KOH solution for 1 h to dissolve the SiO₂. Subsequently, the CNF were treated, after washing with water, in refluxing 65% concentrated nitric acid for 1.5 h, to remove exposed nickel and introduce oxygen-containing functional groups on the CNF surface. Finally, the CNF were washed with demineralized water to neutral pH and ground to a 90–120 μm fraction.

CNF supported catalyst precursors were synthesized by incipient wetness impregnation. Ammonium heptamolybdate (AHM; Sigma-Aldrich, 99.98% trace metals basis), ammonium metatungstate (AMT; Sigma-Aldrich, 99.98% trace metals basis) or a mixture of both salts (molar ratio of Mo:W = 1:3, 1:1 and 3:1) was dissolved in demineralized water. Molar loadings of all catalysts were kept constant at 0.9 mmol metal g_{catalyst}⁻¹. After impregnation, the catalysts were dried overnight at 110 °C.

Catalysts were carburized via the carbothermal reduction, where a heat treatment was applied for 2 h at 900 °C (β = 5 °C/min) under an N₂ flow (50 ml/min). Thus, the carburization was achieved by carbon originating from the support. To avoid contact with air, the carburized catalysts were directly transferred to the glove box workstation, which operated under constant N₂ flow. The catalyst was added to the reaction solvent (dodecane, see below) to transfer it from the glove box workstation to the hydrogenation reactor.

In comparison to the bimetallic carbides, a physical mixture of the monometallic carbides was used. The catalyst precursors of monometallic Mo and W were mixed before the carburization.

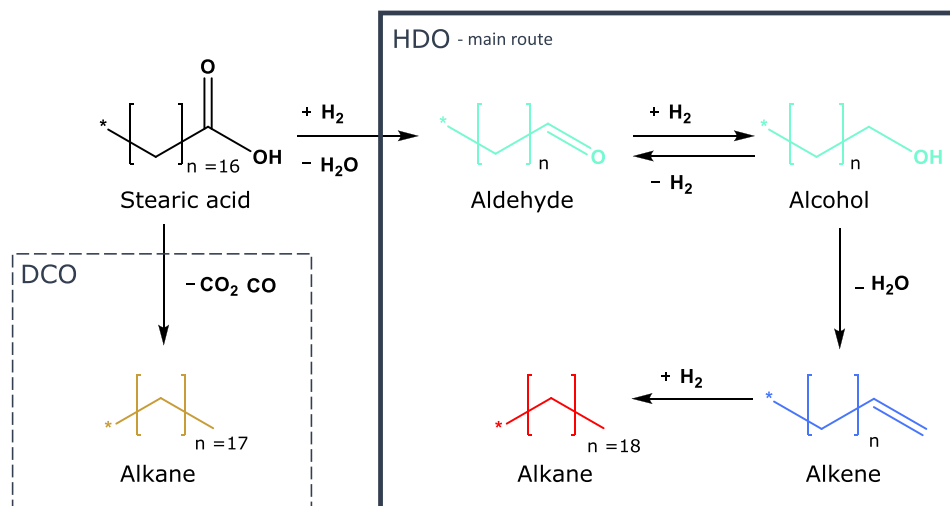
2.2. Characterization

TEM images were acquired using a JEOL JEM-1400 Plus microscope operated at 100 kV. For the sample preparation, ~10 mg of the sample powder was diluted in 1 ml ethanol and deposited on a commercial carbon-coated copper grid. Particle size distributions were obtained by counting 300–400 particles using ImageJ software.

Nitrogen physisorption was used to assess the textural properties of the samples. Nitrogen adsorption/desorption isotherms were recorded at liquid nitrogen temperature using a Micromeritics, Tristar II Plus. Before measurement 100 mg of the sample was degassed at 200 °C for 2 h using a Micromeritics VacPrep 061. For assessing pore volumes, pore sizes and surface area the Brunauer-Emmet-Teller (BET) [25] approach was used.

CO and H₂ chemisorptions were performed on an AutoChem II (Micromeritics). Before a measurement, 200 mg of the catalyst precursor was first flushed for 30 min under He (20 ml/min), then in-situ carburized at 900 °C (β = 5 °C/min) under He (50 ml/min) and cooled to room temperature under He (50 ml/min). For the CO chemisorption, the samples were maintained at 35 °C under He (50 ml/min). Pulses of 0.5 ml 10% CO/He were injected into the He flow. The CO uptake was assessed by TCD and mass spectrometry. The procedure was similar for the H₂ chemisorption, except that 10% H₂/Argon was injected into Argon which was used as carrier gas. For the H site concentration calculation a stoichiometry of Me/H = 1 was assumed. After the chemisorption measurements the samples were analyzed by XRD to assess whether the same crystalline carbide phase was formed during the in-situ carburization as during the ex-situ carburization used for the catalytic experiments. During the transfer from the chemisorption to the XRD workstation the carbide catalysts have been in contact with air.

XRD patterns were recorded on a Bruker D8 Advance using an Lynxeye-XE-T PSD detector and using Cu-Kα_{1,2} radiation (λ = 1.542 Å).



Scheme 1. Reaction pathway of the decarbonylation and decarboxylation (DCO) and hydrodeoxygenation (HDO) of stearic acid.

The measurements were taken from $2\theta = 20^\circ$ to $2\theta = 50^\circ$ with a collection time of 1 s

Temperature Programmed Desorption of ammonia (NH_3 -TPD) was performed on a Micromeritics AutoChem 2920 apparatus. About 100 mg of the catalyst precursor was first flushed for 15 min under He (50 ml/min) and then in-situ carburized at 900°C ($\beta = 5^\circ\text{C}/\text{min}$) under He (50 ml/min). Subsequently, the sample was cooled to 100°C and then 20 pulses of NH_3 with 10% NH_3/He were applied while flowing He (25 ml/min). Afterwards, the sample was heated to 600°C with a ramp of $5^\circ\text{C}/\text{min}$ and held for 30 min to desorb the NH_3 in a pure He flow.

2.3. Catalytic testing

The catalytic reactions were performed in a 100 ml stainless steel Parr autoclave, 4598 Micro batch reactor system. During a standard procedure, the reactor was filled with 250 mg catalyst and 50 ml (Sigma-Aldrich, ReagentPlus®, $\geq 99\%$) (transferred under N_2 as described above), 2 g stearic acid (octadecanoic acid, Sigma-Aldrich, $\geq 95\%$, FCC, FG), 1 g of tetradecane as internal standard (Sigma-Aldrich, $\geq 99\%$). The mixture was twice purged with 30 bar Ar and afterwards flushed with H_2 . Subsequently, the reactor was pressurized to 30 bar of H_2 , heat up to 350°C ($14^\circ\text{C}/\text{min}$) and stirred at 800 rpm. The first sample ($t = 0$ min) was taken when the reactor reached a temperature of 70°C (the melting point of stearic acid). The catalytic reaction

was run for 4 h. A Parr 4878 Automated Liquid Sampler allows collection of filtered liquid samples from the reactor taken at regular time intervals to investigate the product distribution. After taking a sample the pressure was readjusted (when needed) to the setpoint it was found before taking the sample. Prior to GC-FID analysis, $100\ \mu\text{L}$ of the sample was diluted with $900\ \mu\text{L}$ of $\text{CH}_2\text{Cl}_2:\text{MeOH}$ (2:1 v/v%) to dissolve the stearic acid and oxygenate products. Product (normalized) yields were calculated according to (1). The molar carbon balance of the liquid samples of all catalysts is between 80% and 95%.

$$\text{Yield}_{\text{product}x} = \frac{[\text{Product}_x]}{\sum [\text{Product}] + [\text{StearicAcid}]} * 100 \quad (1)$$

With $[\text{Product}_x]$ concentration of a specific product x, $[\text{Product}]$ concentration of all products, $[\text{stearic acid}]$ concentration of stearic acid at a given time.

The total metal based reaction rate (TMR_i) is calculated based on the converted moles of stearic acid per mol of metal ($W + \text{Mo}$). The turnover frequency (TOF) values were based on CO or H_2 chemisorption site concentration and the stearic acid conversion after 1 h. The following equation was used:

$$\text{TOF} = \frac{\text{Molstearicacidconverted}}{\text{Reactiontime(s)} * \text{Molofactivesites}} \quad (2)$$

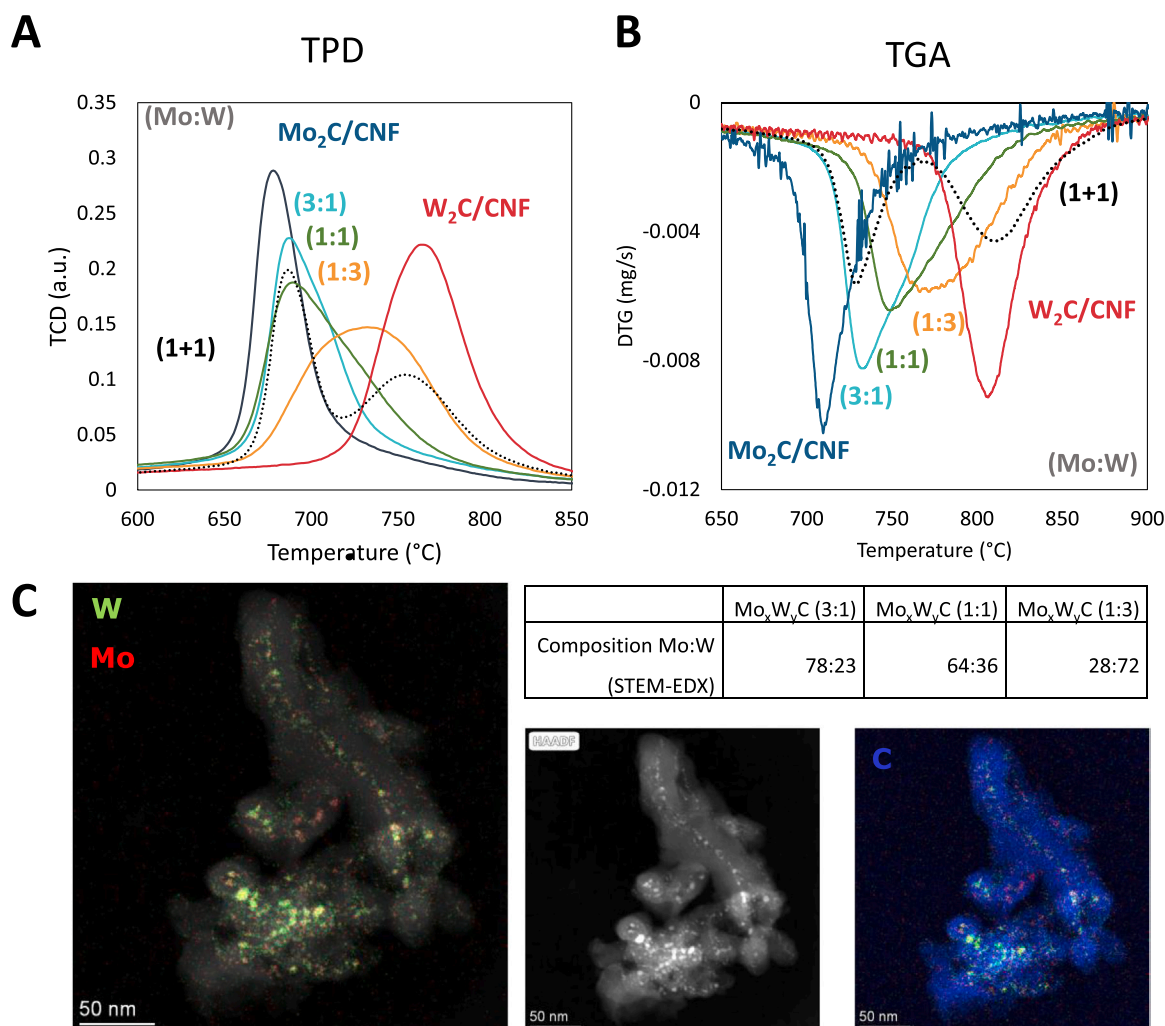


Fig. 1. A: TCD signal representing CO evolution during CR synthesis of monometallic and mixed-metal carbides. B: Comparison of weight change rates during CR synthesis of monometallic and mixed-metal carbides. C: HAADF-STEM image with EDX map overlays of the CR-prepared monometallic and mixed-metal carbides.

3. Results and discussion

3.1. Characterization of bimetallic carbides

In a separate paper, we focused on the synthesis and characterization of CNF supported mixed carbides [26]. Here a brief summary (Fig. 1) of these results is given to understand the most important characteristics of the samples. In addition to that new characterization results relevant for the use of these materials as catalysts for stearic acid deoxygenation will be presented (N_2 physisorption, TEM, $H_2/CO/NH_3$ chemisorption and XRD).

In the carbothermal reduction synthesis, the carbon support containing the metal precursor is heated in an inert atmosphere and the carbon from the support is utilized as reduction and carburization agent. During the reduction of the (Mo/W) oxide to the carbide CO is released measured by TPD-MS and a mass loss was detected by TGA. [26] For the synthesis of mixed metal carbides, the in-situ TPD-MS and TGA analyses of the carburization process can be used to assess whether the carburization of the mixed carbides proceeds in one step or in multiple steps. For our samples it does proceed in one step as shown in Fig. 1a with a carburization temperature (CO release) inbetween those of the monometallic carbides. A physical mixture of the carbide precursors shows again two carburization peaks at the positions of the respective monometallic carbides. This indicates that the mixed carbides consist of a single mixed phase. The CO MS spectra of the Mo carburisation (representative for all samples) can be found in Fig. S1. A similar trend can be observed in Fig. 1B where the thermogravimetric analysis is plotted as DTG (derivate of the mass loss) versus temperature i.e. a single peak representing carburization for the mixed materials. Further investigation of the synthesized carbides with STEM-EDX (Fig. 1C) revealed that they indeed have mixed Mo:W nanoparticles with average compositions matching the W and Mo content of the samples.

3.2. N_2 - physisorption

The textural properties of the support and synthesized catalyst were studied with nitrogen physisorption. The surface area (BET), total pore volume and micropore volume are listed in Table 1. The surface area of parent CNF support is $199 \text{ m}^2/\text{g}$, which is in agreement with earlier studies for CNF made via the same synthesis protocol. [27–29] Among the carbide catalysts no large differences in the textural properties were observed, showing that the Mo or W content does not affect the textural properties of the catalyst. However, the BET surface areas of the catalysts were reduced by ca. 40% when compared to the CNF support. This is partly due to the loading of the support with metal carbides (assuming the carbides are non porous). In addition, in the parent CNF some amorphous carbon can be present (causing the higher micropore volume observed in Table 1) which can be lost during the carburization process. Moreover, pore blocking by the metal-carbide can occur which all can explain the decrease in BET surface area. [30–32].

Table 1

Textural properties of CNF, Mo_2C/CNF , W_2C/CNF and mixed MoW-carbides, as determined by N_2 -physisorption.

	BET surface area (m^2/g)	Pore volume (cm^3/g)	Micropore volume (cm^3/g)
CNF	199	0.4	$2.0 \cdot 10^{-2}$
Mo_2C/CNF	131	0.3	$1.8 \cdot 10^{-3}$
W_2C/CNF	102	0.3	$3.4 \cdot 10^{-3}$
Mo_xW_yC/CNF (1:1)	114	0.3	$5.3 \cdot 10^{-3}$
Mo_xW_yC/CNF (1:3)	133	0.3	$9.7 \cdot 10^{-3}$
Mo_xW_yC/CNF (3:1)	144	0.3	$1.1 \cdot 10^{-3}$

3.2.1. TEM

The structure and particle size of CNF supported carbide catalysts were further examined by transmission electron microscope (TEM) as depicted in Fig. 2. The carbide particles appeared as spherical shaped particles supported on the fibers. The carbide nanoparticles size of the synthesized carbides is typically 4–6 nm with averages between 4.3 and 5.7 nm as indicated in Fig. 2. All mixed carbides thus have similar particle sizes in line with those reported earlier [21,27].

3.3. CO and H_2 chemisorption

In order to get more insight into the number and nature of the (re) active sites CO/H_2 -chemisorption (for metallic sites) and NH_3 -TPD experiments (for acids sites) were performed. H_2 -chemisorption [33,34] and especially CO chemisorption [33–38] are commonly used to probe the carbidic sites. Please note that it is essential to perform chemisorption without exposure of the samples to air since that might (surface) oxidize the carbide. Therefore, we carburized our samples in-situ. Table 2 shows the measured CO and H site densities. The CO uptake for all carbide catalysts was in the range of 44–52 $\mu\text{mol}/\text{g}$. The pure Mo-carbide had the lowest (44.4 $\mu\text{mol}/\text{g}$) and the pure W-carbide had the highest CO uptake (51.7 $\mu\text{mol}/\text{g}$). The mixed carbide catalysts showed values intermediate to those of the pure carbides. For the H_2 -chemisorption the W-carbide (30.2 $\mu\text{mol}/\text{g}$) had the highest uptake followed by the Mo-carbide (22.8 $\mu\text{mol}/\text{g}$) but here the mixed carbides showed the lowest site densities (15–21 $\mu\text{mol}/\text{g}$). In addition, to H_2 -chemisorption, the measured site densities were lower compared to the CO site concentration. Clearly, both probe gases do not measure the same sites. In addition, also the ratio between these sites is varying among samples since the ratio of the CO to H site densities varied between 1.7 and 3.1 (Table 2).

In addition, we also probed the acidic sites of the fresh monometallic Mo and W carbide catalysts by NH_3 -TPD. No desorption could be detected showing that the amount of acid sites on these materials is insignificant (Fig. S2).

3.3.1. XRD

In order to assess the nature of the carbide phases formed during the in-situ carburization in the chemisorption equipment, the catalysts were investigated with XRD directly after the (CO and H_2) chemisorption measurements (Fig. 3). The signals at $2\theta = 28^\circ$ and $2\theta = 43^\circ$ represent the (002) and (101) reflections of the CNF [29]. Further, the XRD pattern displays the characteristic peaks of the hexagonal semi carbide phases (W_2C , Mo_2C) indicating that all catalysts were fully carburized and have the same crystal structure regardless of their composition. For the Mo_2C these peaks are at $2\theta = 34.4^\circ$, 37.8° and 39.4° (PDF 79–0744) and for W_2C at $2\theta = 34.5^\circ$, 38.0° and 39.5° (PDF 89–2371). Though the position of the reflections match those with expected values the intensity of the reflections did not. It is expected that $I_{\text{carbide}}/I_{\text{CNF}}$ increases with increasing W-loading since the molar loading is constant, and tungsten is a much heavier scatterer than molybdenum. The (3:1) and (1:1) sample fall within the expected trend, however the (1:3) sample does not (Fig. 3) which we can not explain at this moment.

Nevertheless, these XRD results are identical to the post synthesis XRD measurements showing that small differences in carburization (smaller scale) set-up do not affect the carburization process.

3.4. Catalytic performance

The catalytic performance (selectivity and activity) of the prepared catalysts was evaluated for the stearic acid hydrodeoxygenation in a batch reactor (350°C and 30 bar H_2).

Fig. 4 presents product yields over time for the monometallic carbides and the three bimetallic carbides with different ratios (Mo:W: 3:1, 1:1 and 1:3). The two main possible pathways (Scheme 1) of stearic acid towards hydrocarbons are (1) the direct decarboxylation (DCO)

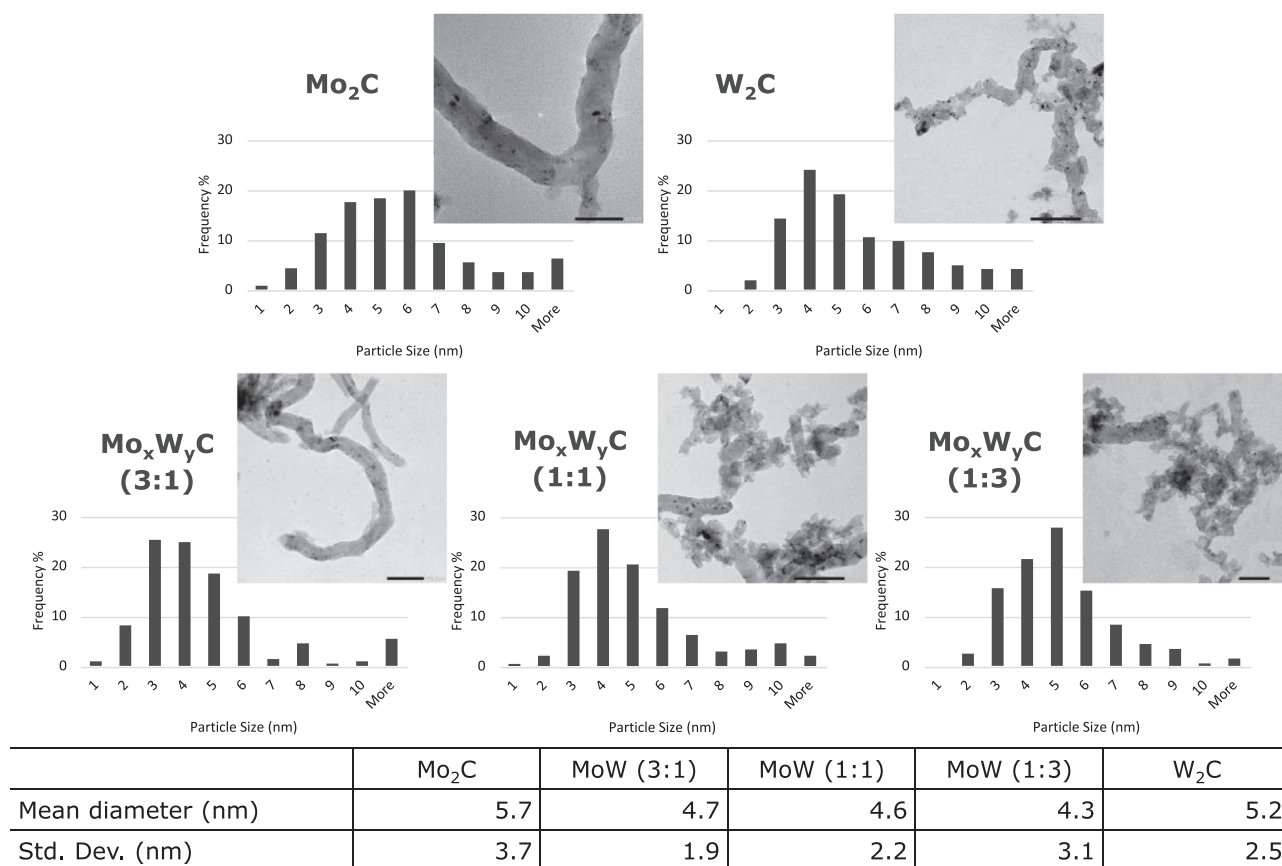


Fig. 2. TEM images and particle size distribution of monometallic Mo and W and bimetallic MoW-carbide catalysts.

Table 2

CO and H site concentration ($\mu\text{mol/g}$) of Mo₂C/CNF, W₂C/CNF and three mixed MoW-carbides with different Mo:W ratios.

($\mu\text{mol/g}$)	Mo ₂ C	Mo _x W _y C (3.1)	Mo _x W _y C (1.1)	Mo _x W _y C (1.3)	W ₂ C
CO site concentration ($\mu\text{mol/g}$)	44.4 \pm 2.7	47.8 \pm 4.8	46.7 \pm 5.2	48.6 \pm 3.9	51.7 \pm 5.2
H site concentration ($\mu\text{mol/g}$)	22.8 \pm 10.4	15.2 \pm 3.0	19.2 \pm 6.6	21.2 \pm 1.3	30.2 \pm 1.0
Ratio CO/H	1.9	3.1	2.4	2.3	1.7

*Uncertainties based on the duplicate measurements of the chemisorption.

involving C-C cleavage yielding C17 alkanes and (2) the hydrodeoxygenation (HDO) yielding C18 products. The formation of DCO products (C17) is observed for all carbide catalysts but with low selectivity (~10%). All the carbide catalysts showed high selectivity towards products of the HDO pathway (oxygenates, saturated and unsaturated C18). However, there were substantial differences in the product distribution profiles. The Mo carbide reached high yields towards oxygenates (max 38 mol% after 1 h), while the W-carbide more selectively produced alkenes (max 26 mol% in 2 h) as the main intermediate product. The bimetallic systems simultaneously produced significant amounts of both, alkenes and oxygenates as intermediate products. Formation of higher C36-esters via condensation of oxygenates was observed to be a minor reaction pathway over all the tested carbide catalysts.

To make a clearer comparison of the catalytic behaviour between the different carbide catalysts, the yield as a function of the conversion for oxygenates, alkenes and alkanes over the mono and bimetallic carbides was plotted in Fig. 5. The monometallic Mo carbide catalyst yielded maximum oxygenates of 40% (C18-oxy) at conversion levels of 80 mol% and the monometallic W carbide yielded maximum alkene of 28% (C18-alkene) at 70 mol% conversions. The bimetallic carbides reached oxygenates and alkenes yields in between that of the monometallic carbide,

where the bimetallic system with higher Mo mol.% also reached higher oxygenates yields while the system with higher W wt% resulted in higher yields of alkenes. Interestingly, the bimetallic catalysts retained highly selective towards the alkene at higher stearic acid conversions (20–40 mol% alkenes at > 80% conversion), while the monometallic W-carbide showed lower alkene yield at higher conversions (10 mol% alkenes at 90% conversion). Another interesting observation was made for the physical mixture which behaves in terms of selectivity similar to the 1:1 bimetallic carbide system. In addition a control experiment on CNF was performed and is shown in Fig. S3. The activity of pure CNF was neglectable.

The initial activity (in the 1st hour, corresponds to 30–40% conversion of SA) for all catalysts is reported in Table 3. The activity is expressed as both total metal based rate (TMR_i, converted moles of stearic acid per mol W and/or Mo) and turn-over-frequency (TOF_i, converted moles of stearic acid per mol surface sites) using the site concentration from CO (TOF_{i,CO}) and H₂-chemisorption (TOF_{i,H2}), see Table 2. The TMR_i shows that the monometallic Mo-carbide was the most active, being almost two times more active than the monometallic W-carbide. The bimetallic carbides were comparable in activity to the W-carbide. To compare the intrinsic activity of the carbides either CO chemisorption or H chemisorption can be used for assessing that

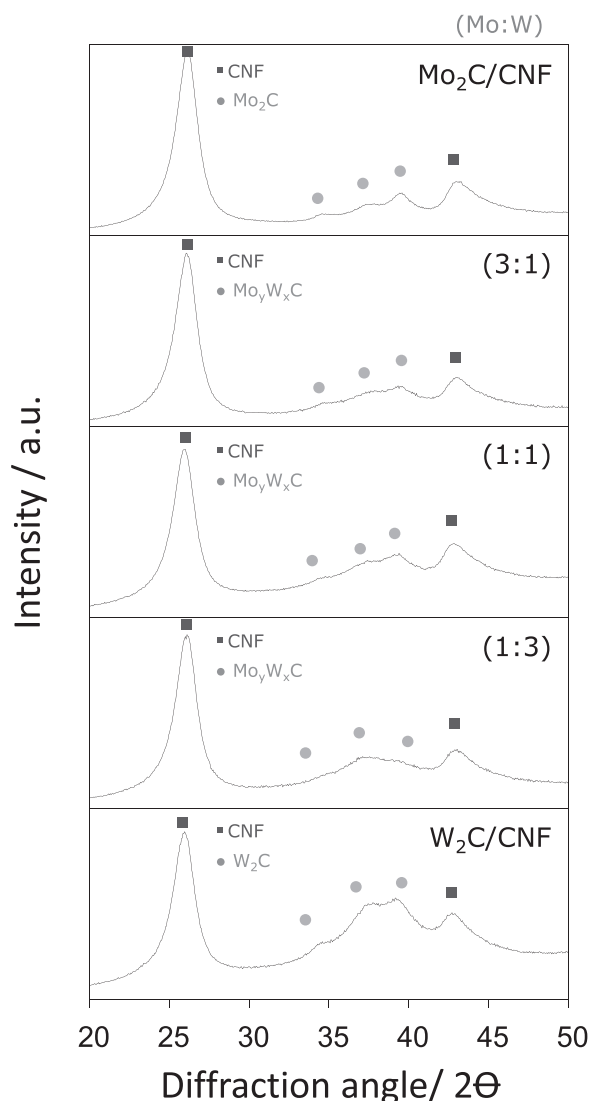


Fig. 3. XRD pattern of monometallic carbide catalyst samples and bimetallic carbide catalyst samples post chemisorption analysis.

activity. Fig. 6 displays the TOF as function of Mo content for the different sample based on both methods of chemisorption. In addition, Fig. 6 shows that there is no clear relation between the Mo content and TOF_{CO} while there seems to be a linear relationship between Mo content and TOF_{H_2} . Therefore TOF_{H_2} seems to be a better indicator for the role of Mo than TOF_{CO} .

4. Overall discussion

4.1. Characterization

Depending on the carburization conditions different textural and structural properties e.g. complex crystal structures and different phase compositions (carbide versus oxycarbides) may emerge. [39] For that reason it is important to establish these properties among a set of different carbide catalysts and to enable the comparison of the different catalysts, since e.g. crystal structures, [27,40] phase compositions [23] and particle sizes [39] can affect the catalytic activity and selectivity. First, the BET surface area and pore volume measured by N_2 physisorption did not show significant differences among the carbide catalysts. The XRD measurements revealed that the synthesis via the carbothermal reduction for both the monometallic carbides and bimetallic carbide samples results in a metal carbide phase with a hexagonal

crystal structure. Since no other oxides or oxycarbide phase was detected we conclude that a fully carburized phase (Me_2C , $\text{Me}=\text{Mo}$ or W) with the same structure was obtained for all catalysts. TEM images of the bimetallic and monometallic carbide catalysts were taken to examine the particle size. The average nanoparticle size for all catalysts (Fig. 2) was found to be in a similar range of 4–6 nm which is in agreement with similarly prepared carbide catalysts [21,23,27]. For the bimetallic catalysts the interaction between Mo and W had been demonstrated by the changes in carburization temperature [26]. The formation of mixed metal carbides was proven by HAADF-STEM analysis which revealed that the carburization process results in individual nanoparticles containing both Mo and W in a composition that is on average close to those of their respective bulk ratio. [26] Thus, we conclude that the bimetallic catalysts consist of nanoparticles containing both Mo and W but without discernible difference in terms of surface area, crystal phase and nanoparticle size compared to the monometallic samples. However, by performing H_2 and CO chemisorption (Table 2) to probe the carbidic sites of the prepared carbide catalysts [33,41], differences between the monometallic and bimetallic carbide could be established. The CO site concentration of supported Mo_2C was slightly lower ($44 \mu\text{mol/g}$) in comparison to the W_2C ($52 \mu\text{mol/g}$). The bimetallic carbides have CO site densities in-between that of the pure metal carbides ($47\text{--}48 \mu\text{mol/g}$). In contrast, the results of the H_2 -chemisorption show that the bimetallic carbides have lower site densities ($15\text{--}22 \mu\text{mol/g}$) than the monometallic carbides (23 and $30 \mu\text{mol/g}$ for the Mo-carbide and W-carbide respectively). As a result, the CO/ H_2 ratios are similar for the monometallic carbide catalysts (1.7–1.9) but increase for the bimetallic carbides (2.3–3.1). The fact that this ratio increases for the bimetallic carbides, while the CO site concentration for bimetallic catalyst is as would be expected based on the results of Mo-carbide and W-carbide, shows that the decrease in H_2 site concentration for the bimetallic catalysts is not simply due to a difference in particle size, which is also in agreement with the TEM analysis. The decrease in H_2 sites for the bimetallic catalyst thus appears to be a direct consequence of the formation of the mixed metal carbides. We therefore suggest that the molecular adsorption of CO on the metal centers of the carbide surface [42,43] is not significantly affected by the alloying while the ensembles of sites required for the dissociative adsorption of H_2 [44] are diminished due to the alloying.

4.2. Catalytic performance

The catalytic selectivity and activity of the different carbide catalysts were evaluated for the hydrodeoxygenation of stearic acid in a batch reactor (350°C and 30 bar H_2). As mentioned earlier, the deoxygenation of stearic acid can occur either via the decarboxylation (and decarbonylation) pathway (DCO) yielding hydrocarbon chains with one carbon atom less than the reactant or via the hydrodeoxygenation (HDO) resulting in hydrocarbons with same chain lengths. Direct decarboxylation and/or decarbonylation of stearic acid into C17 hydrocarbons has previously been reported to occur over WO_x and MoO_x species. [22,23] We observed only small amounts ($\sim 10\%$) of DCO products in the reaction mixture, suggesting that no or low amounts of oxide species were present in the catalyst. This is in agreement with $\beta\text{-Mo}_2\text{C}$ as the dominant crystal phase and the absence of metal oxide species (MoO_3 and WO_3/WO_2 crystalline phases) revealed by the XRD analysis. Additionally, the absence of acid sites revealed by $\text{NH}_3\text{-TPD}$ further demonstrates the absence of significant amount of oxy-carbide surface sites on the in-situ prepared catalyst.

For the HDO reaction pathway over Mo and W carbide catalysts, it has been reported that bi-functional properties are present in the form of a metallic hydrogenation and acidic dehydration functionality [45]. These acid sites are the result of some form of oxygen introduction to the carbide surface which can either be introduced after the carburization by exposure to air (passivation) [46] or originates from in-situ generation of $\text{O}^* \text{-Me}_2\text{C}$ species [45] when the catalyst is exposed to oxygen

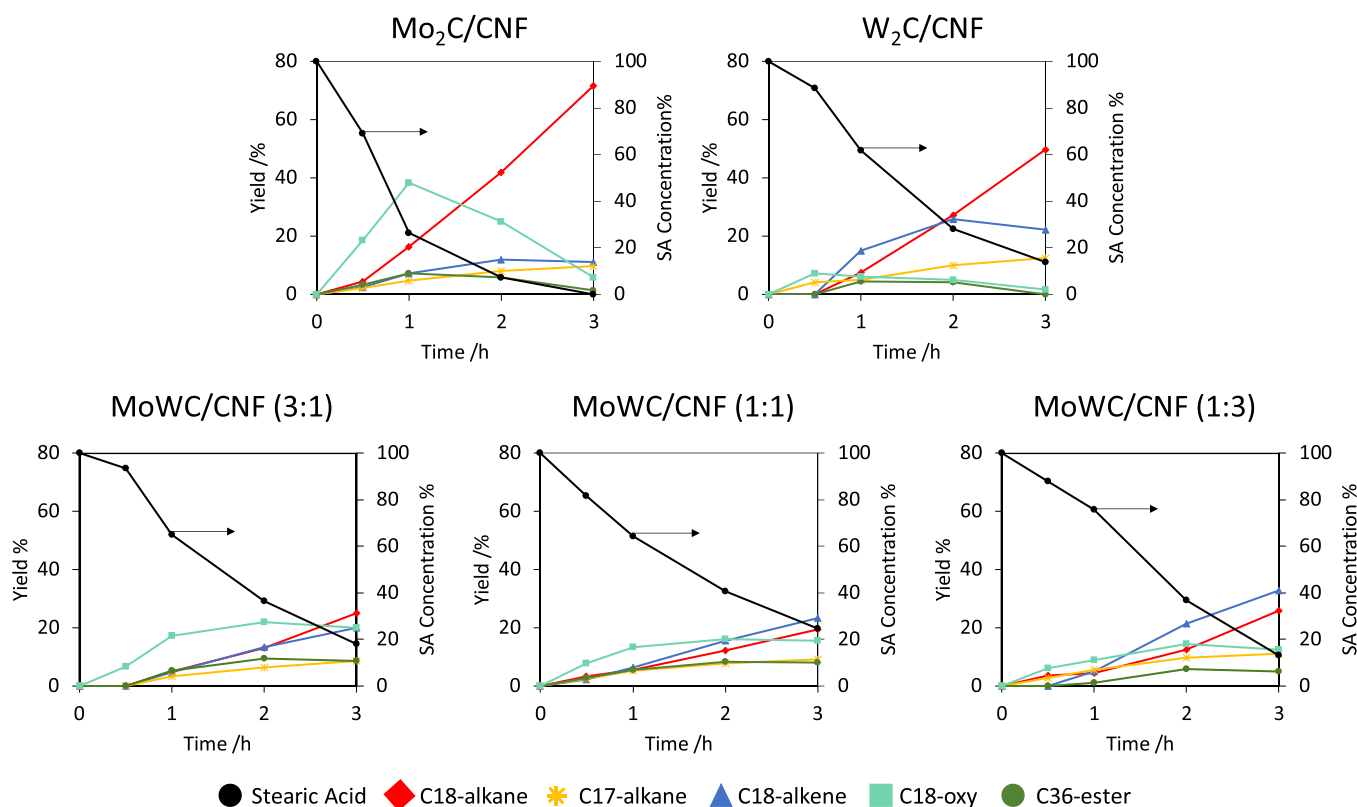


Fig. 4. Stearic acid concentration and product distribution over time of $\text{Mo}_2\text{C}/\text{CNF}$, $\text{W}_2\text{C}/\text{CNF}$, bimetallic Mo:W carbides with ratio of 3:1, 1:1 and 1:3. (250 mg catalysts, 2 g stearic acid, 350 °C, 50 ml solvent, 30 bar H_2).

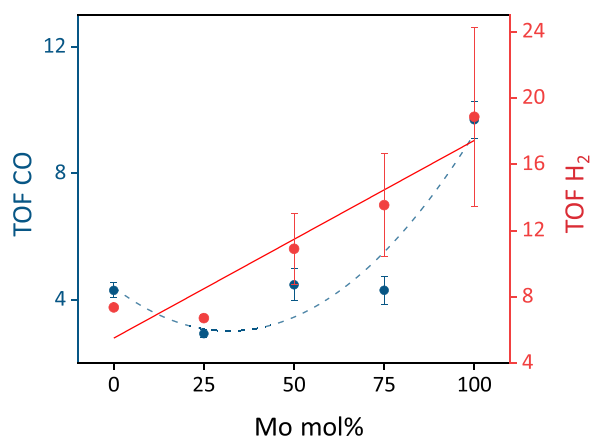


Fig. 5. Oxygenates, alkene and alkane yield vs conversion of monometallic and bimetallic carbide systems during stearic acid hydrodeoxygenation (250 mg catalysts, 2 g stearic acid, 350 °C, 50 ml solvent, 30 bar H_2).

from the reactant or to the formed water. [47,48] Since on our Mo and W carbide catalysts no NH_3 desorption and thus no acid sites could be detected, our results agree with the latter explanation. For the bimetallic MoW carbide catalysts these bi-functional properties also remain, since all the catalysts preferred HDO route yielding C18 products. However, a marked difference in product composition over time was observed between the W-carbide, bimetallic-carbides and Mo-carbide catalysts. A clear difference in the main intermediate was observed with high yields of oxygenates (aldehyde and alcohol, ~40 mol%) observed up to high conversion with Mo-carbide while high yields of unsaturated C18 (~25 mol%) were found for W-carbide at high conversion level. This can be explained by a difference in the relative rates of acid hydrogenation

Table 3

Activity of the carbide catalysts based on weight (TMR_i), CO chemisorption ($\text{TOF}_{i,\text{CO}}$) and H_2 chemisorption ($\text{TOF}_{i,\text{H}_2}$).

Catalyst	Mo_2C	$\text{Mo}_x\text{W}_y\text{C}$ (3:1)	$\text{Mo}_x\text{W}_y\text{C}$ (1:1)	$\text{Mo}_x\text{W}_y\text{C}$ (1:3)	W_2C
$\text{TMR}_i \cdot 10^2$ (min^{-1}) ^a	9.6	4.6	4.7	3.2	4.9
$\text{TOF}_{i,\text{CO}}$ (min^{-1}) ^b	9.7	4.3	4.5	2.9	4.3
$\text{TOF}_{i,\text{H}_2}$ (min^{-1}) ^c	18.9	13.5	10.9	6.7	7.4

^aConverted moles of stearic acid per mol W and/or Mo after 1 h

^bTurnover frequency based on CO chemisorption after 1 h

^cTurnover frequency based on H_2 chemisorption after 1 h

and alcohol dehydration between Mo-carbide and W-carbide. For the Mo-carbide the hydrogenation of the acid proceeds relatively fast compared to the dehydration rate to the alkene, this results in increased levels of oxygenates as the main intermediate. In comparison, for the W-carbide the hydrogenation of the acid to oxygenates occurs slower than the dehydration toward the alkene, which results in elevated levels of alkenes as the main intermediate. The higher dehydration activity of W-carbide is then likely related to higher acidity. The difference between the Mo and the W carbide has earlier been explained by their differences in oxophilic properties (and hydrogenation power). [21,33,35,49,50] The more oxophilic W-carbide is more likely to generate acid sites upon exposure to oxygen or in reactions with oxygenated compounds. The observation that with the W-carbide no alkenes are present at the initial stage of the reaction (Figs. 4 and 5) suggests that it takes some time until sufficient amounts of acidic sites are formed.

The mixed Mo:W carbides reached oxygenate and alkene yields in between that of the monometallic carbides. The bimetallic systems with a higher Mo wt% have higher selectivity towards oxygenates, while the bimetallic systems with higher W content are more selective for alkenes.

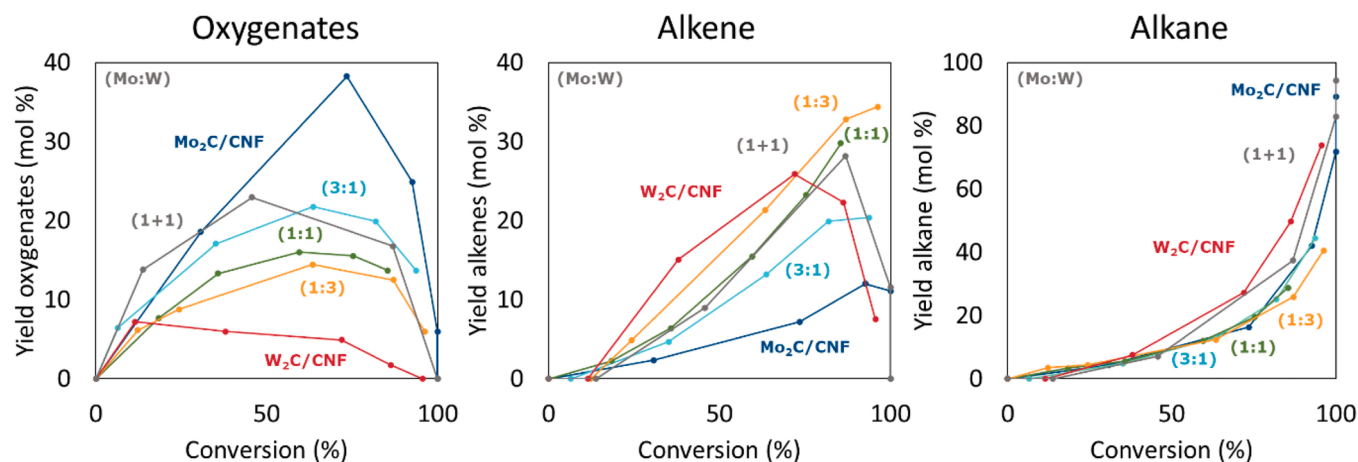


Fig. 6. CO and H₂ site concentration based TOF versus Mo mol%. (Standard deviation based on duplicate measurements of the chemisorption).

Interestingly, we observed that the bimetallic catalysts with a ratio of 1:3 Mo to W retain high selectivity towards the alkene at higher stearic acid conversions (35 mol% alkenes at > 80% conversion), while the monometallic W-carbide showed lower alkene yield at higher conversions (10 mol% alkenes at 90% conversion). Hence, the addition of molybdenum to W carbide catalysts delays full hydrogenation of the alkenes. This may appear counterintuitive since we have established that Mo is the better hydrogenation catalyst. However, Fig. 5 also shows that higher alkane yields are obtained over monometallic W-carbide at each measured conversion level. This is the result of the much higher intermediate alkene concentration with the monometallic W-carbide. Reducing the dehydration activity by the addition of Mo can thus result in a shift of maximum alkene production to higher conversion levels.

Interestingly, the physical mixture (1 + 1) and the bimetallic system (1:1) do behave similarly (see Fig. 5). The oxygenates, alkenes and alkane yields of the physical mixture and the bimetallic system are nearly identical at each conversion level. Thus, irrespective whether the carbide catalysts do contain mixed (Mo_xW_yC_z) nanoparticles or monometallic carbides (Mo₂C + W₂C), the catalytic selectivity of both catalysts is similar. These results suggest that mixed Mo-W carbide active centers either have catalytic properties in between those of Mo and W or that the nanoparticles consist of ensembles still mainly Mo-carbide or W-carbide in nature.

Besides the differences in product distribution also the catalytic activity of the monometallic and bimetallic catalysts was compared. It should be mentioned that comparing the activities is not straightforward considering the bifunctional nature of the catalyst and the mentioned possibility of the in-situ formation of new active sites. Hence, we limit ourselves to a comparison of the initial activity in which mainly the activity of the catalyst with respect to the acid hydrogenation is evaluated (Table 3). On a total metal basis, the Mo-carbide was found to be the most active catalyst (9.6 min⁻¹) followed by the W-carbide catalyst (4.9 min⁻¹) and the mixed metal carbides are found to be the least active (3.2–4.7 min⁻¹). To get more insight into the reason for the decreased activity of the bimetallic catalysts we also compared the site based activities (Table 3 & Fig. 6) using the site concentration from both CO and H₂ chemisorption (Table 2). For the monometallic catalyst, the TOF_i based on either CO or H₂ shows that the Mo-carbide has a higher site based initial activity than W-carbide. These trends are consistent with previous reports. [21,23] Since the ratio between CO and H₂ uptake is nearly the same for the monometallic carbides (1.7–1.9), either can be used for a comparative evaluation of the site based activity. We demonstrate that this is not the case for bimetallic catalysts for which the CO/H₂ ratio differs from the monometallic carbides (2.3–3.1). We already concluded that changes in CO/H₂ ratio is due to a decrease in H₂ site concentration when forming the mixed metal carbide phase. Thus,

the decreased activity on a total metal basis correlates to a decrease in the H₂ site concentration. Fig. 6 reveals that for the TOF_{i,H2} a linear relation is obtained with the Mo content of the catalyst. In other words, the sites probed by H₂ in the bimetallic catalyst act as a linear combination of those present in pure Mo-carbide and W-carbide sites. On the other hand, using the TOF_{i,CO} values would lead to the conclusion that the surface of bimetallic particles behaves more like the monometallic W-carbide, which we know is not the case since we have established that the bimetallic catalysts have a behavior which is in-between the pure metal carbides with respect to their product formation. Given these results and the fact that the initial reaction step is in fact a hydrogenation reaction, i.e. requiring hydrogen activation, we suggest that H₂ based activity is the best descriptor for the TOF_i.

5. Conclusion

The catalytic performance of MoW mixed metal carbide catalysts in the stearic acid deoxygenation has been studied. Both monometallic carbides (W-carbide and Mo-carbide) and the bimetallic carbides (MoW-carbide with different ratios) preferred the HDO pathway over the DCO pathway, which is consistent with the presence of a pure metal carbide phase without strong acid sites according to XRD and ammonia TPD. The Mo:W ratio was found to influence the product yield towards either oxygenates or alkenes in the HDO pathway. The more Mo-rich samples have a higher yield towards oxygenates, while the more W-rich samples have higher yields towards the alkene intermediate. The behaviour of the 1:1 MoW-carbide was found to be similar to a physical mixture of monometallic Mo and W-carbides. Based on the characterization with TEM and both CO and H₂ chemisorption it was shown that the formation of a bimetallic phase results in a decrease in H₂ site concentration. The linear relation of the H₂ site based activity together with the evolution of the product distribution as function of the Mo content of the catalyst, suggests that the H₂ site concentration is a better descriptor for site base activity than the CO site concentration. Therefore, we conclude that although the formation of a bimetallic carbide results in loss of hydrogenation sites, the properties of the monometallic catalyst (having higher hydrogenation activity for Mo-carbide and higher dehydration activity for the W-carbide) are proportionally transferable to the bimetallic systems.

CRediT authorship contribution statement

Marlene Führer designed and performed the experiments. Harry Bitter and Tomas van Haasterecht contributed to the design and the interpretation. Marlene Führer wrote the draft of the manuscript. All authors revised the paper.

Declaration of Competing Interest

The authors declare that they have no known competing financial interests or personal relationships that could have appeared to influence the work reported in this paper.

Data Availability

Data will be made available on request.

Acknowledgement

Acknowledgement is made to the Dutch Research Council (NWO) for financial support (grant number NOW 729.004.002). The authors gratefully thank Susan Witte for assistance with GC-FID measurements. We also would like to thank Sebastian Haben for performing the NH₃-TPD analysis and Raghavendra Meena for the discussion regarding the CO and H₂ dissociation on the carbide surface.

Appendix A. Supporting information

Supplementary data associated with this article can be found in the online version at [doi:10.1016/j.cattod.2023.114108](https://doi.org/10.1016/j.cattod.2023.114108).

References

- [1] M. Führer, T. van Haasterecht, J. Bitter, *Catal. Sci. Technol.* (2020).
- [2] A. Mehdad, R.E. Jentoft, F.C. Jentoft, *J. Catal.* 351 (2017) 161–173.
- [3] A. Szymanska-Kolasa, M. Lewandowski, C. Sayag, D. Brodzki, G. Djega-Mariadassou, *Catal. Today* 119 (2007) 35–38.
- [4] P. Da Costa, J.-L. Lemberon, C. Potvin, J.-M. Manoli, G. Perot, M. Breyse, G. Djega-Mariadassou, *Catal. Today* 65 (2001) 195–200.
- [5] R.B. Levy, M. Boudart, *Science* 181 (1973) 547–549.
- [6] I. Kojima, E. Miyazaki, Y. Inoue, I. Yasumori, *J. Catal.* (U. S.) 59 (1979).
- [7] A. Kumar, S. Phadke, A. Bhan, *Catal. Sci. Technol.* 8 (2018) 2938–2953.
- [8] J.S. Lee, S. Locatelli, S.T. Oyama, M. Boudart, *J. Catal.* 125 (1990) 157–170.
- [9] H.A. Al-Megren, T. Xiao, S.L. Gonzalez-Cortes, S.H. Al-Khowaiter, M.L. Green, *J. Mol. Catal. A: Chem.* 225 (2005) 143–148.
- [10] S. Masoumi, A.K. Dalai, *Energy Convers. Manag.* 231 (2021), 113834.
- [11] H. Chen, Q. Wang, X. Zhang, L. Wang, *Fuel* 159 (2015) 430–435.
- [12] L. Zhao, K. Fang, D. Jiang, D. Li, Y. Sun, *Catal. Today* 158 (2010) 490–495.
- [13] S. Zhang, C. Shi, B. Chen, Y. Zhang, Y. Zhu, J. Qiu, *C. Au, Catal. Today* 258 (2015) 676–683.
- [14] S. Izhar, M. Yoshida, M. Nagai, *Electrochim. Acta* 54 (2009) 1255–1262.
- [15] A.A. Smirnov, Z. Geng, S.A. Khromova, S.G. Zavarukhin, O.A. Bulavchenko, A. Saraev, V.V. Kaichev, D.Y. Ermakov, V.A. Yakovlev, *J. Catal.* 354 (2017) 61–77.
- [16] H. Shao, E.L. Kugler, W. Ma, D.B. Dadyburjor, *Ind. Eng. Chem. Res* 44 (2005) 4914–4921.
- [17] M.V. Iyer, L.P. Norcio, E.L. Kugler, D.B. Dadyburjor, *Ind. Eng. Chem. Res* 42 (2003) 2712–2721.
- [18] M.V. Iyer, L.P. Norcio, A. Punnoose, E.L. Kugler, M.S. Seehra, D.B. Dadyburjor, *Top. Catal.* 29 (2004) 197–200.
- [19] C.C. Tran, Y.L. Hang, M. Garcia-Perez, S. Kaliaguine, *Catal. Sci. Technol.* 9 (2019) 1387–1397.
- [20] Q. Fu, B.X. Peng, J. Masa, Y.T. Chen, W. Xia, W. Schuhmann, M. Muhler, *Chemelectrochem* 7 (2020) 983–988.
- [21] D.R. Stellwagen, J.H. Bitter, *Green. Chem.* 17 (2015) 582–593.
- [22] S.A.W. Hollak, R.W. Gosselink, D.S. van Es, J.H. Bitter, *ACS Catal.* 3 (2013) 2837–2844.
- [23] R.W. Gosselink, D.R. Stellwagen, J.H. Bitter, *Carbohydr. Res.* 52 (2013) 5089–5092.
- [24] M. Snåre, I. Kubickova, P. Mäki-Arvela, K. Eränen, D.Y. Murzin, *Ind. Eng. Chem. Res* 45 (2006) 5708–5715.
- [25] P. Sinha, A. Datar, C. Jeong, X. Deng, Y.G. Chung, L.-C. Lin, *J. Phys. Chem. C.* 123 (2019) 20195–20209.
- [26] M. Führer, T. van Haasterecht, J.H. Bitter, Submitted (2022).
- [27] L.S. Macedo, R.R. Oliveira, T. van Haasterecht, V. Teixeira da Silva, H. Bitter, *Appl. Catal. B: Environ.* 241 (2019) 81–88.
- [28] M.L. Toebes, E.M.P. van Heeswijk, J.H. Bitter, A.J. van Dillen, K.P. de Jong, *Carbon* 42 (2004) 307–315.
- [29] A.L. Jongerius, R.W. Gosselink, J. Dijkstra, J.H. Bitter, P.C.A. Bruijninx, B. M. Weckhuysen, *ChemCatChem* 5 (2013) 2964–2972.
- [30] L. Souza Macedo, V. Teixeira da Silva, J.H. Bitter, *ChemEngineering* 3 (2019) 24.
- [31] A.S. Rocha, V.T. da Silva, A.C. Faro Jr, *Appl. Catal. A: Gen.* 314 (2006) 137–147.
- [32] I.T. Ghampson, C. Sepúlveda, R. Garcia, J.G. Fierro, N. Escalona, W.J. DeSisto, *Appl. Catal. A: Gen.* 435 (2012) 51–60.
- [33] C.-C. Tran, D. Akmach, S. Kaliaguine, *Green. Chem.* (2020).
- [34] J.S. Lee, K.H. Lee, J.Y. Lee, *J. Phys. Chem.* 96 (1992) 362–366.
- [35] A. Mehdad, R.E. Jentoft, F.C. Jentoft, *Catal. Today* 323 (2019) 112–122.
- [36] W.S. Lee, Z. Wang, W. Zheng, D.G. Vlachos, A. Bhan, *Catal. Sci. Technol.* 4 (2014) 2340–2352.
- [37] P. Da Costa, J.L. Lemberon, C. Potvin, J.M. Manoli, G. Perot, M. Breyse, G. Djega-Mariadassou, *Catal. Today* 65 (2001) 195–200.
- [38] J.-S. Choi, G. Bugli, G. Djéga-Mariadassou, *J. Catal.* 193 (2000) 238–247.
- [39] A. Shrestha, X.T. Gao, J.C. Hicks, C. Paolucci, *Chem. Mater.* 33 (2021) 4606–4620.
- [40] Q. Yang, K. Sun, Y. Xu, Z. Ding, R. Hou, *Appl. Catal. A: Gen.* 630 (2022), 118455.
- [41] J. Zhu, E.A. Uslamin, N. Kosinov, E.J. Hensen, *Catal. Sci. Technol.* 10 (2020) 3635–3645.
- [42] T. Wang, Y.W. Li, J. Wang, H. Jiao, S. Wang, *J. Phys. Chem. C.* 116 (2012) 6340–6348.
- [43] W. Wu, Z. Wu, C. Liang, X. Chen, P. Ying, C. Li, *J. Phys. Chem. B* 107 (2003) 7088–7094.
- [44] S. Posada-Pérez, F. Viñes, R. Valero, J.A. Rodriguez, F. Illas, *Surf. Sci.* 656 (2017) 24–32.
- [45] M.M. Sullivan, A. Bhan, *ACS Catal.* 6 (2016) 1145–1152.
- [46] M. Führer, T. van Haasterecht, J.H. Bitter, *Chem. Commun.* (2022), <https://doi.org/10.1039/D2CC05322E>.
- [47] M.M. Sullivan, A. Bhan, *J. Catal.* 344 (2016) 53–58.
- [48] P.M. Mortensen, H.W.P. de Carvalho, J.-D. Grunwaldt, P.A. Jensen, A.D. Jensen, *J. Catal.* 328 (2015) 208–215.
- [49] C.-C. Tran, O. Mohan, A. Banerjee, S.H. Mushrif, S. Kaliaguine, *Energy Fuels* 34 (2020) 16265–16273.
- [50] A. Mehdad, R.E. Jentoft, F.C. Jentoft, *J. Catal.* 347 (2017) 89–101.